HAMOR, M. J. & HAMOR, T. A. (1978*a*). *Acta Cryst.* B**34**, 863–866.
HAMOR, M. J. & HAMOR, T. A. (1978*b*). *Acta Cryst.* B**34**, 2994–2997.
KRONEBUSCH, P., GLEASON, W. B. & BRITTON, D. (1976). *Cryst. Struct. Commun.* **5**, 17–20.
LESSER, D. P., DE VRIES, A., REED, J. W. & BROWN, G. H. (1975). *Acta Cryst.* B**31**, 653–658.
PEDERSEN, B. F. (1975). *Acta Cryst.* B**31**, 2931–2933.
ROBERTSON, G. B. (1961). *Nature (London)*, **191**, 593–594.
RØMMING, C., SEIP, H. M. & AANESEN ØYMO, I.-M. (1974). *Acta Chem. Scand. Ser. A.* **28**, 507–514, and references therein.
SCHMID, E. D. & BROSA, B. (1972). *J. Chem. Phys.* **56**, 6267–6268.
SCHOMAKER, V. & TRUEBLOOD, K. N. (1968). *Acta Cryst.* B**24**, 63–76.
SHELDRICK, G. M. (1976). *SHELX. Program for Crystal Structure Determination.* Univ. of Cambridge, England.

Acta Cryst. (1980). B**36**, 1406–1418

Chiral Mono-*N*-Substituted Primary Amides. I. Molecular Packing Modes

BY S. WEINSTEIN AND L. LEISEROWITZ

Departments of Organic Chemistry and Structural Chemistry, The Weizmann Institute of Science, Rehovot, Israel

(*Received* 17 *November* 1979; *accepted* 2 *January* 1980)

Abstract

Molecular packing modes of RCONHCH(CH_3)Ar, in which R are alkyl and Ar are aromatic residues, were determined and analysed in terms of molecular interactions to be used for the interpretation of chiral recognition phenomena involving these amides. The cell constants of a number of the amides as well as the crystal structures of (*R*)-*N*-trifluoroacetyl-1-(1-naphthyl)ethylamine, (*R*)- and (*RS*)-*N*-acetyl-1-(1-naphthyl)ethylamine were determined. Various molecular interactions are analysed and it is shown that the hydrogen-bonded 5 Å translation stack is particularly stable, sufficiently for the arrangement to be partially conserved in the melt.

1. Introduction

Our interest in chiral recognition stems from current work on the separation of enantiomers by chromatography (Weinstein, Feibush & Gil-Av, 1976) and crystallization (Lahav, Laub, Gati, Leiserowitz & Ludmer, 1976) and the resulting need to understand and control stereoselectivity. Chiral recognition involves differential interaction between a molecule, or an ensemble of molecules, with two enantiomorphs and can be expressed quantitatively by the difference in the stability constants of their diastereomeric association.

Here we are concerned with chiral secondary amides RCONHCH(CH_3)Ar with varying R and Ar groups, and the interactions between molecules within this series. In these systems, where the constituents are so similar in their chemical structure and the components contain an aromatic group, Ar, the stereoselective effects observed are relatively strong (Weinstein, Feibush & Gil-Av, 1976) and they are therefore suitable for the study of chiral recognition on the molecular level. The solid state has been chosen for this study since it represents minimum-energy arrangements of molecules. Thus, the relative stabilities of various interactions between chiral molecules can be recognized and evaluated.

In this work, the molecular packing modes of a series of enantiomerically pure and of racemic *N*-acyl-1-arylethylamines were determined from their cell constants and from detailed structure determination of three compounds. Evidence is produced for retention in the melt of some of the packing features observed in the crystalline state. In addition, an analysis of preferred conformations and intermolecular arrangements as carried out by energy computations is presented.

A model for chiral recognition based on the preferred modes of packing of these compounds derived here is presented in a separate publication (Weinstein, Leiserowitz & Gil-Av, 1980). It explains, on the molecular level, the stereoselectivity observed in both the solid and liquid states.

0567-7408/80/061406-13$01.00

2. X-ray structure determination of (*R*)-*N*-trifluoroacetyl-1-(1-naphthyl)ethylamine [(*R*)-TFA NAPH] and (*R*)- and (*RS*)-*N*-acetyl-1-(1-naphthyl)ethylamine [(*R*)-ACE NAPH and (*RS*)-ACE NAPH]

2.1. *Data collection*

The cell dimensions of (*R*)-TFA NAPH, (*R*)-ACE NAPH and (*RS*)-ACE NAPH (Table 1) were derived by least squares from high-order reflections ($\sin\theta/\lambda > 0{\cdot}5$ Å^{-1}) measured on a Nonius CAD-3 diffractometer with Mo $K\alpha$ radiation. The intensities were collected on the diffractometer with Mo $K\alpha$ radiation and a graphite monochromator. The diffractometer was controlled by a Varian 620/L-100 computer. The details of the data collection and processing are given in Table 2.

2.2. *Structure solution and refinement*

The structures were solved with *MULTAN* (Germain, Main & Woolfson, 1971). *E* maps computed with the models which had the highest figure of merit revealed the molecular skeletons.

The C, N, O and F atoms were refined isotropically and then anisotropically by full-matrix least squares. Next, all H atoms, except those of the methyl groups, were inserted in chemically reasonable positions, and the methyl H atoms were located on difference maps. Parameters were refined until convergence, no parameter shift in the final least-squares cycle being $>0{\cdot}1\sigma$. Scattering factors were taken from *International Tables for X-ray Crystallography* (1962). The details and results of the refinement are presented in Table 3. The atomic coordinates, as labelled below, are listed in Table 4, and bond lengths and angles in Tables 5 and 6.*

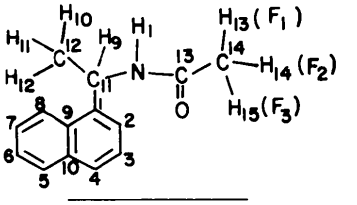

* Lists of structure factors, intermolecular distances and anisotropic thermal parameters have been deposited with the British Library Lending Division as Supplementary Publication No. SUP 35094 (20 pp.). Copies may be obtained through The Executive Secretary, International Union of Crystallography, 5 Abbey Square, Chester CH1 2HU, England.

Table 2. *Intensity measurement and processing*

	(*R*)-TFA NAPH	(*R*)-ACE NAPH	(*RS*)-ACE NAPH
Crystal dimensions (mm)	0·1 × 0·2 × 0·8	0·2 × 0·2 × 0·6	0·8 × 0·2 × 0·4
Reciprocal-lattice vector parallel to φ axis [*hkl*]	[001]	[$\bar{1}$02]	[001]
Maximum θ angle (°)	27	27	27
Scanning mode	$\theta/2\theta$	$\theta/2\theta$	$\theta/2\theta$
θ step scan for reflection scan (°)	0·01	0·01	0·02
Step-scan time for intensity and background (s)	0·4, 0·2	0·5, 0·2	0·4, 0·2
Number of monitor reflections	4	4	4
Monitor reflection interval	100	100	100
Number of reflections measured	2928	2964	2804
Number of unique reflections	1503	1375	1399
Number of unobserved reflections for which $F_o^2 < 2\sigma(F_o^2)$	290	248	487
The match between equivalent reflections R'*	0·042	0·044	0·087
Variation in the computed absorption factor A†	0·97–0·99	0·98–0·99	0·97–0·98

* $R' = \sum_{ij}(F_{ij} - \bar{F}_j)^2/\sum_{ij}F_{ij}^2$ where $\bar{F}_j = \sum_i w_{ij}F_{ij}/\sum_i w_{ij}$ is the weighted average of the jth group of i symmetry-equivalent reflections. F_{ij} is the individual value of each reflection in the group and w_{ij} is the corresponding weight.

† The crystal X-ray absorption factors, A, were computed by the Gaussian quadrature method (Coppens, Leiserowitz & Rabinovich, 1965).

Table 1. *Crystal data of* RCONHCH(CH_3)Ar

Name	Compound *R*	Compound Ar*	*R* or *RS*	m.p. (°C)	Space group	*a* (Å)	*b* (Å)	*c* (Å)	β (°)	*Z*	D_c (Mg m^{-3})	H-bonding motif: Symmetry element	H-bonding motif: Axis
ACE PHE†	CH_3	C_6H_5	*R*	102	$P4_12_12$	6·8	6·8	41·9		8	1·13	2_1 axis	*a* + *b*
TFA PHE	CF_3	C_6H_5	*R*	92	$P2_1$	12·3	8·3	5·2	92	2	1·35	translation	*c*
TFA PHE	CF_3	C_6H_5	*RS*	65–6	$P2_1/c$	8·2	5·3	24·0	98	4	1·37	translation	*b*
LAU PHE	$nC_{11}H_{23}$	C_6H_5	*R*	62	$P2_12_12$	4·9	7·6	26·1		2	1·04	translation	*a*
PIVA PHE	$C(CH_3)_3$	C_6H_5	*S*	118	$P4_12_12$	11·6	11·6	19·7		8	1·03	4_1 axis	*c*
PIVA PHE	$C(CH_3)_3$	C_6H_5	*RS*	98	$P2_1/c$	16·3	9·5	15·7	108	8	1·17		
ACE NAPH‡	CH_3	$C_{10}H_7$	*R*	152	$P2_1$	12·982 (10)	9·552 (6)	4·816 (2)	100·14 (3)	2	1·20	translation	*c*
ACE NAPH‡	CH_3	$C_{10}H_7$	*RS*	126–8	$Pca2_1$	7·635 (3)	17·457 (12)	8·957 (7)		4	1·18	glide	*c*
ACE NAPH	CH_3	$C_{10}H_7$	*RS*	126–8	$Pna2_1$	17·4	13·8	4·9		4	1·20	translation	*c*
TFA NAPH‡	CF_3	$C_{10}H_7$	*R*	114	$P2_12_12_1$	19·592 (7)	12·666 (6)	5·149 (1)		4	1·39	translation	*c*
TFA NAPH	CF_3	$C_{10}H_7$	*RS*	112–4	$P2_1/a$	9·2	14·1	10·2	86·5	4	1·31	glide	*a*
BUT NAPH	nC_3H_7	$C_{10}H_7$	*R*	115–7	$P2_1$	11·4	4·9	14·0	104	2	1·02	translation	*b*
LAU NAPH§	$nC_{11}H_{23}$	$C_{10}H_7$	*R*	98–9			5					translation	*b*
LAU NAPH	$nC_{11}H_{23}$	$C_{10}H_7$	*RS*	89–91	$Pca2_1$	8·0	29·6	9·2		4	1·08	glide	*c*
LAU NAPHBr	$nC_{11}H_{23}$	$C_{10}H_6Br$	*R*	100	$P2_1$	30·9	4·9	7·7	84	2	1·25	translation	*b*
PIVA NAPH	$C(CH_3)_3$	$C_{10}H_7$	*S*	129	$P2_12_12_1$	19·3	8·7	19·0		8	1·05	pseudo 4_1 axis	
PIVA NAPH	$C(CH_3)_3$	$C_{10}H_7$	*RS*	137–8	$P\bar{1}$ or $P1$	11·8	9·5	15·3	$\alpha = 92{\cdot}9$ $\beta = 72{\cdot}1$ $\gamma = 66{\cdot}3$	4	1·13		

* C_6H_5 = phenyl, $C_{10}H_7$ = 1-naphthyl, $C_{10}H_6Br$ = 1-(4-bromonaphthyl).

† This compound resolved spontaneously on crystallization.

‡ The cell constants, λ(Mo $K\alpha_1$) = 0·70926 Å, were determined by least squares (see § 2.1.); values in parentheses are e.s.d.'s.

§ The 5 Å axis was unambiguously determined from an oscillation photograph of a cluster of aligned needles.

Table 3. *Crystal-structure refinement*

The quantity minimized was $\sum w[(kF_o)^2 - F_c^2]^2$.

	(*R*)-TFA NAPH	(*R*)-ACE NAPH	(*RS*)-ACE NAPH
Number of parameters refined	220	189	144
Number of reflections used in the refinement	1202	1181	1039
Number of reflections given zero weight believed to have extinction errors	8	9	8
R (including unobserved reflections)	0·060	0·081	0·089
$r = \frac{\sum w[(kF_o)^2 - F_c^2]^2}{\sum wk^4F_o^4}$	0·005	0·013	0·020
Goodness of fit $\left\{\frac{\sum w[(kF_o)^2 - F_c^2]^2}{n-p}\right\}^{1/2}$	2·98	2·47	2·67

n = number of observations
p = number of parameters

Table 4. *Fractional atomic coordinates* ($\times 10^4$ *for* C, N, O *and* F *and* $\times 10^3$ *for* H) *and their e.s.d.'s*

(*a*) (*R*)-*N*-Trifluoroacetyl-1-(1-naphthyl)ethylamine

	x	*y*	*z*
C(1)	5923 (2)	4972 (4)	2263 (9)
C(2)	6198 (2)	4321 (5)	4078 (10)
C(3)	6706 (3)	4658 (7)	5803 (11)
C(4)	6935 (3)	5651 (7)	5715 (12)
C(5)	6928 (3)	7406 (6)	3652 (16)
C(6)	6692 (3)	8083 (6)	1758 (19)
C(7)	6191 (3)	7748 (5)	36 (15)
C(8)	5937 (2)	6763 (4)	203 (10)
C(9)	6163 (2)	6031 (4)	2077 (9)
C(10)	6679 (2)	6379 (5)	3853 (11)
C(11)	5390 (2)	4586 (4)	386 (9)
C(12)	5281 (4)	3407 (5)	293 (19)
C(13)	4338 (2)	5378 (4)	−1105 (9)
C(14)	3652 (2)	5869 (4)	−409 (10)
N(1)	4733 (2)	5118 (3)	854 (8)
O(1)	4475 (2)	5278 (4)	−3389 (7)
F(1)	3556 (2)	6008 (4)	2071 (8)
F(2)	3160 (1)	5265 (3)	−1274 (11)
F(3)	3569 (2)	6779 (3)	−1592 (10)
H(1)	460 (3)	521 (5)	229 (14)
H(2)	603 (3)	364 (5)	441 (15)
H(3)	691 (3)	427 (6)	725 (17)
H(4)	732 (3)	599 (4)	681 (14)
H(5)	725 (3)	768 (4)	490 (13)
H(6)	685 (3)	885 (5)	161 (13)
H(7)	602 (3)	826 (6)	−131 (17)
H(8)	558 (3)	653 (4)	−113 (14)
H(9)	550 (2)	488 (4)	−131 (11)
H(10)	492 (3)	318 (5)	−129 (14)
H(11)	516 (3)	315 (6)	178 (17)
H(12)	569 (3)	308 (5)	−33 (12)

Table 4 (*cont.*)

(*b*) (*R*)-*N*-Acetyl-1-(1-naphthyl)ethylamine

	x	*y*	*z*
C(1)	3015 (3)	9147 (5)	2482 (10)
C(2)	3522 (4)	8352 (7)	774 (12)
C(3)	2994 (5)	7274 (6)	−931 (14)
C(4)	1984 (5)	6978 (6)	−847 (12)
C(5)	363 (4)	7467 (7)	1001 (13)
C(6)	−176 (5)	8216 (8)	2645 (14)
C(7)	324 (4)	9295 (6)	4331 (13)
C(8)	1348 (4)	9610 (6)	4202 (11)
C(9)	1934 (4)	8870 (6)	2565 (10)
C(10)	1428 (4)	7761 (6)	854 (10)
C(11)	3562 (3)	10301 (6)	4300 (11)
C(12)	4766 (4)	10267 (9)	4723 (19)
C(13)	2933 (3)	12682 (6)	4796 (10)
C(14)	2531 (5)	14011 (6)	3353 (12)
N(1)	3177 (3)	11675 (5)	3161 (8)
O(1)	3020 (3)	12570 (0)	7378 (7)
H(1)	306 (4)	1190 (5)	97 (12)
H(2)	422 (4)	852 (6)	40 (13)
H(3)	337 (4)	676 (6)	−215 (11)
H(4)	158 (4)	627 (6)	−218 (11)
H(5)	7 (5)	680 (6)	−9 (12)
H(6)	−85 (5)	798 (6)	276 (12)
H(7)	−9 (4)	986 (6)	575 (13)
H(8)	167 (4)	1029 (6)	572 (12)
H(9)	332 (4)	1021 (5)	665 (12)
H(10)	500 (4)	1045 (6)	262 (12)
H(11)	502 (4)	924 (6)	528 (13)
H(12)	498 (4)	1111 (6)	590 (12)
H(13)	262 (4)	1409 (6)	155 (13)
H(14)	277 (4)	1484 (7)	412 (13)
H(15)	179 (4)	1415 (6)	394 (13)

(*c*) (*RS*)-*N*-Acetyl-1-(1-naphthyl)ethylamine*

	x	*y*	*z*
C(1)	966 (6)	2687 (3)	922 (10)
C(2)	−162 (8)	2970 (4)	−158 (11)
C(3)	−1557 (9)	2527 (5)	−716 (10)
C(4)	−1771 (9)	1789 (6)	−208 (14)
C(5)	−873 (12)	714 (4)	1488 (16)
C(6)	158 (14)	430 (4)	2518 (17)
C(7)	1492 (10)	886 (4)	3175 (15)
C(8)	1743 (9)	1602 (3)	2607 (11)
C(9)	724 (8)	1929 (3)	1490 (10)
C(10)	−680 (9)	1472 (4)	893 (12)
C(11)	2522 (7)	3139 (3)	1415 (10)
C(12)	4226 (7)	2828 (4)	804 (10)
C(13)	1790 (8)	4487 (3)	1970 (9)
C(14)	1923 (8)	5300 (3)	1378 (11)
N(1)	2418 (6)	3958 (2)	1045 (9)
O(1)	1188 (6)	4327 (2)	3209 (0)
H(1)	295	413	9
H(2)	6	353	−60
H(3)	−234	274	−153
H(4)	−280	152	−63
H(5)	−182	42	119
H(6)	−8	−10	296
H(7)	232	61	396
H(8)	280	193	299
H(9)	260	310	255
H(10)	432	284	−17
H(11)	442	231	110
H(12)	521	307	124
H(13)	176	530	21
H(14)	84	563	188
H(15)	312	553	167

* The H-atom coordinates of (*RS*)-ACE NAPH were not refined; therefore derived parameters do not have e.s.d.'s.

Table 5. *Bond lengths* (Å)

(*a*) (*R*)-*N*-Trifluoroacetyl-1-(1-naphthyl)ethylamine

C(1)–C(2)	1·358 (7)	C(1)–C(11)	1·505 (6)
C(2)–C(3)	1·401 (8)	C(11)–C(12)	1·509 (8)
C(3)–C(4)	1·336 (12)	C(11)–N(1)	1·473 (5)
C(4)–C(10)	1·422 (9)	C(13)–N(1)	1·313 (6)
C(5)–C(10)	1·393 (9)	C(13)–C(14)	1·523 (7)
C(5)–C(6)	1·379 (11)	C(13)–O(1)	1·213 (6)
C(6)–C(7)	1·388 (11)	C(14)–F(1)	1·303 (7)
C(7)–C(8)	1·346 (8)	C(14)–F(2)	1·308 (6)
C(8)–C(9)	1·410 (7)	C(14)–F(3)	1·314 (7)
C(9)–C(10)	1·431 (6)		
C(1)–C(9)	1·424 (7)		
C(2)–H(2)	0·94 (7)	C(11)–H(9)	0·97 (6)
C(3)–H(3)	0·98 (8)	C(12)–H(10)	1·11 (7)
C(4)–H(4)	1·04 (6)	C(12)–H(11)	0·87 (8)
C(5)–H(5)	0·97 (6)	C(12)–H(12)	0·96 (6)
C(6)–H(6)	1·02 (6)	N(1)–H(1)	0·79 (7)
C(7)–H(7)	1·01 (8)		
C(8)–H(8)	1·02 (6)		

(*b*) (*R*)-*N*-Acetyl-1-(1-naphthyl)ethylamine

C(1)–C(2)	1·370 (8)	C(1)–C(11)	1·506 (7)
C(2)–C(3)	1·417 (8)	C(11)–C(12)	1·541 (7)
C(3)–C(4)	1·349 (9)	C(11)–N(1)	1·475 (7)
C(4)–C(10)	1·401 (9)	C(13)–N(1)	1·317 (7)
C(5)–C(10)	1·425 (8)	C(13)–C(14)	1·497 (8)
C(5)–C(6)	1·351 (9)	C(13)–O(1)	1·233 (6)
C(6)–C(7)	1·399 (9)		
C(7)–C(8)	1·375 (7)		
C(8)–C(9)	1·383 (8)		
C(9)–C(10)	1·429 (7)		
C(1)–C(9)	1·435 (6)		
C(2)–H(2)	0·97 (6)	C(11)–H(9)	1·23 (6)
C(3)–H(3)	0·96 (6)	C(12)–H(10)	1·12 (6)
C(4)–H(4)	1·01 (5)	C(12)–H(11)	1·05 (6)
C(5)–H(5)	0·87 (6)	C(12)–H(12)	1·00 (6)
C(6)–H(6)	0·91 (6)	C(14)–H(13)	0·90 (6)
C(7)–H(7)	1·08 (6)	C(14)–H(14)	0·91 (6)
C(8)–H(8)	1·01 (5)	C(14)–H(15)	1·06 (6)
		N(1)–H(1)	1·06 (6)

(*c*) (*RS*)-*N*-Acetyl-1-(1-naphthyl)ethylamine

C(1)–C(2)	1·387 (11)	C(1)–C(11)	1·493 (8)
C(2)–C(3)	1·409 (11)	C(11)–C(12)	1·512 (8)
C(3)–C(4)	1·376 (14)	C(11)–N(1)	1·471 (7)
C(4)–C(10)	1·405 (14)	C(13)–N(1)	1·331 (9)
C(5)–C(10)	1·434 (12)	C(13)–C(14)	1·518 (9)
C(5)–C(6)	1·310 (17)	C(13)–O(1)	1·234 (8)
C(6)–C(7)	1·421 (14)		
C(7)–C(8)	1·363 (10)		
C(8)–C(9)	1·390 (11)		
C(9)–C(10)	1·439 (10)		
C(1)–C(9)	1·429 (9)		
C(2)–H(2)	1·08	C(11)–H(9)	1·02
C(3)–H(3)	1·01	C(12)–H(10)	0·87
C(4)–H(4)	0·99	C(12)–H(11)	0·95
C(5)–H(5)	0·92	C(12)–H(12)	0·94
C(6)–H(6)	1·03	C(14)–H(13)	1·05
C(7)–H(7)	1·06	C(14)–H(14)	1·10
C(8)–H(8)	1·04	C(14)–H(15)	1·03
		N(1)–H(1)	0·99

Table 6. *Bond angles* (°)

(*a*) (*R*)-*N*-Trifluoroacetyl-1-(1-naphthyl)ethylamine

C(2)–C(1)–C(9)	119·1 (4)	C(2)–C(1)–C(11)	121·4 (4)
C(9)–C(1)–C(11)	119·5 (4)	C(1)–C(2)–C(3)	122·3 (6)
C(1)–C(2)–H(2)	123 (4)	C(3)–C(2)–H(2)	115 (4)
C(2)–C(3)–C(4)	120·2 (6)	C(2)–C(3)–H(3)	129 (4)
C(4)–C(3)–H(3)	111 (4)	C(3)–C(4)–C(10)	121·0 (5)
C(3)–C(4)–H(4)	128 (3)	C(10)–C(4)–H(4)	111 (3)
C(6)–C(5)–C(10)	121·1 (6)	C(6)–C(5)–H(5)	118 (4)
C(10)–C(5)–H(5)	121 (4)	C(5)–C(6)–C(7)	119·9 (7)
C(5)–C(6)–H(6)	123 (4)	C(7)–C(6)–H(6)	117 (4)
C(6)–C(7)–C(8)	120·3 (7)	C(6)–C(7)–H(7)	118 (4)
C(8)–C(7)–H(7)	122 (4)	C(7)–C(8)–C(9)	122·4 (5)
C(7)–C(8)–H(8)	118 (3)	C(9)–C(8)–H(8)	119 (3)
C(1)–C(9)–C(8)	124·1 (4)	C(1)–C(9)–C(10)	118·7 (4)
C(8)–C(9)–C(10)	117·2 (4)	C(4)–C(10)–C(5)	122·1 (5)
C(4)–C(10)–C(9)	118·7 (5)	C(5)–C(10)–C(9)	119·1 (5)
C(1)–C(11)–C(12)	116·1 (5)	C(1)–C(11)–N(1)	110·7 (4)
C(1)–C(11)–H(9)	108 (3)	C(12)–C(11)–N(1)	109·5 (4)
C(12)–C(11)–H(9)	112 (3)	N(1)–C(11)–H(9)	99 (3)
C(11)–C(12)–H(10)	111 (3)	C(11)–C(12)–H(11)	113 (5)
C(11)–C(12)–H(12)	109 (4)	H(10)–C(12)–H(11)	112 (6)
H(10)–C(12)–H(12)	100 (5)	H(11)–C(12)–H(12)	111 (6)
C(14)–C(13)–N(1)	116·2 (4)	C(14)–C(13)–O(1)	117·8 (4)
N(1)–C(13)–O(1)	126·0 (4)	C(13)–C(14)–F(1)	114·4 (4)
C(13)–C(14)–F(2)	109·4 (4)	C(13)–C(14)–F(3)	111·0 (4)
F(1)–C(14)–F(2)	107·8 (5)	F(1)–C(14)–F(3)	108·5 (5)
F(2)–C(14)–F(3)	105·3 (4)	C(11)–N(1)–C(13)	120·3 (4)
C(11)–N(1)–H(1)	121 (4)	C(13)–N(1)–H(1)	119 (4)

(*b*) (*R*)-*N*-Acetyl-1-(1-naphthyl)ethylamine

C(2)–C(1)–C(9)	119·3 (5)	C(2)–C(1)–C(11)	121·8 (4)
C(9)–C(1)–C(11)	118·8 (4)	C(1)–C(2)–C(3)	121·1 (5)
C(1)–C(2)–H(2)	126 (3)	C(3)–C(2)–H(2)	113 (3)
C(2)–C(3)–C(4)	120·6 (6)	C(2)–C(3)–H(3)	118 (3)
C(4)–C(3)–H(3)	121 (3)	C(3)–C(4)–C(10)	120·6 (5)
C(3)–C(4)–H(4)	121 (3)	C(10)–C(4)–H(4)	118 (3)
C(6)–C(5)–C(10)	122·1 (6)	C(6)–C(5)–H(5)	122 (4)
C(10)–C(5)–H(5)	116 (4)	C(5)–C(6)–C(7)	119·7 (6)
C(5)–C(6)–H(6)	120 (4)	C(7)–C(6)–H(6)	120 (4)
C(6)–C(7)–C(8)	119·2 (6)	C(6)–C(7)–H(7)	120 (3)
C(8)–C(7)–H(7)	121 (3)	C(7)–C(8)–C(9)	123·2 (5)
C(7)–C(8)–H(8)	113 (3)	C(9)–C(8)–H(8)	123 (3)
C(1)–C(9)–C(8)	124·1 (5)	C(1)–C(9)–C(10)	118·3 (5)
C(8)–C(9)–C(10)	117·6 (4)	C(4)–C(10)–C(5)	121·9 (5)
C(4)–C(10)–C(9)	120·1 (5)	C(5)–C(10)–C(9)	118·0 (5)
C(1)–C(11)–C(12)	115·1 (5)	C(1)–C(11)–N(1)	109·9 (4)
C(1)–C(11)–H(9)	108 (2)	C(12)–C(11)–N(1)	109·7 (5)
C(12)–C(11)–H(9)	107 (2)	N(1)–C(11)–H(9)	106 (2)
C(11)–C(12)–H(10)	108 (2)	C(11)–C(12)–H(11)	108 (3)
C(11)–C(12)–H(12)	103 (3)	H(10)–C(12)–H(11)	105 (5)
H(10)–C(12)–H(12)	107 (5)	H(11)–C(12)–H(12)	124 (4)
C(14)–C(13)–N(1)	116·3 (4)	C(14)–C(13)–O(1)	120·3 (5)
N(1)–C(13)–O(1)	123·5 (5)	C(13)–C(14)–H(13)	115 (4)
C(13)–C(14)–H(14)	119 (4)	C(13)–C(14)–H(15)	104 (3)
H(13)–C(14)–H(14)	103 (6)	H(13)–C(14)–H(15)	121 (5)
H(14)–C(14)–H(15)	92 (5)	C(11)–N(1)–C(13)	121·9 (4)
C(11)–N(1)–H(1)	121 (3)	C(13)–N(1)–H(1)	117 (3)

(*c*) (*RS*)-*N*-Acetyl-1-(1-naphthyl)ethylamine

C(2)–C(1)–C(9)	119·9 (6)	C(2)–C(1)–C(11)	120·8 (6)
C(9)–C(1)–C(11)	119·1 (6)	C(1)–C(2)–C(3)	121·4 (7)
C(1)–C(2)–H(2)	119	C(3)–C(2)–H(2)	119
C(2)–C(3)–C(4)	119·1 (8)	C(2)–C(3)–H(3)	120
C(4)–C(3)–H(3)	121	C(3)–C(4)–C(10)	122·1 (8)
C(3)–C(4)–H(4)	114	C(10)–C(4)–H(4)	124
C(6)–C(5)–C(10)	123·3 (9)	C(6)–C(5)–H(5)	117
C(10)–C(5)–H(5)	119	C(5)–C(6)–C(7)	120·7 (8)
C(5)–C(6)–H(6)	120	C(7)–C(6)–H(6)	118
C(6)–C(7)–C(8)	117·4 (10)	C(6)–C(7)–H(7)	117
C(8)–C(7)–H(7)	125	C(7)–C(8)–C(9)	124·5 (7)
C(7)–C(8)–H(8)	119	C(9)–C(8)–H(8)	116
C(1)–C(9)–C(8)	124·3 (6)	C(1)–C(9)–C(10)	118·5 (7)
C(8)–C(9)–C(10)	117·1 (6)	C(4)–C(10)–C(5)	124·3 (8)
C(4)–C(10)–C(9)	118·9 (7)	C(5)–C(10)–C(9)	116·8 (8)
C(1)–C(11)–C(12)	112·8 (5)	C(1)–C(11)–N(1)	113·9 (5)
C(1)–C(11)–H(9)	107	C(12)–C(11)–N(1)	108·3 (5)
C(12)–C(11)–H(9)	107	N(1)–C(11)–H(9)	107
C(11)–C(12)–H(10)	115	C(11)–C(12)–H(11)	112
C(11)–C(12)–H(12)	112	H(10)–C(12)–H(11)	107
H(10)–C(12)–H(12)	109	H(11)–C(12)–H(12)	100
C(14)–C(13)–N(1)	114·0 (7)	C(14)–C(13)–O(1)	123·4 (6)
N(1)–C(13)–O(1)	122·5 (6)	C(13)–C(14)–H(13)	110
C(13)–C(14)–H(14)	107	C(13)–C(14)–H(15)	110
H(13)–C(14)–H(14)	108	H(13)–C(14)–H(15)	111
H(14)–C(14)–H(15)	110	C(11)–N(1)–C(13)	123·7 (7)
C(11)–N(1)–H(1)	118	C(13)–N(1)–H(1)	118

(Each ring H atom was given the number of the C atom to which it is attached.)

2.3. *Molecular shapes*

Equations for the best planes through the naphthyl and amide groups are given in Table 7. The chiral C atom in the three structures lies very close to the planes of the amide and naphthyl groups. The planes of the naphthyl and amide groups are perpendicular to each other in (*R*)-TFA NAPH and (*R*)-ACE NAPH (89 and 90° respectively). The corresponding angle in (*RS*)-ACE NAPH is 77°.

There is no free rotation around the C(14)—CO bond in all three structures. In the chiral structure the average torsion angle Ψ [H—C(14)—C(13)—N] (derived from the torsion angles Ψ_1, Ψ_2, Ψ_3 of the three individual H atoms by taking the average of Ψ_1, $\Psi_2 - 120°$ and $\Psi_3 - 240°$) is 8·6° for (*R*)-ACE NAPH, and for (*R*)-TFA NAPH the average Ψ angle [F—C(14)—C(13)—N] is 5° (Table 8). The corresponding angle in the racemate (*RS*)-ACE NAPH is 32·2°. According to an analysis (Hagler, Leiserowitz & Tuval, 1976) of the conformational properties of the acetamide group, the conformation in which Ψ is 0° is the most commonly observed, indicating a higher stability for this conformation.

Table 7. *Description of best planes*

Group	Equation of best plane*	$\left[\frac{(\sum \Delta^2)}{n-1}\right]^{1/2}$†
	(*R*)-TFA NAPH	
Naphthyl	$-13{\cdot}8540x + 3{\cdot}8410y + 3{\cdot}2889z + 5{\cdot}5652 = 0$	0·007
Amide	$8{\cdot}0855x + 11{\cdot}5360y - 0{\cdot}0563z - 9{\cdot}7237 = 0$	0·002
	(*R*)-ACE NAPH	
Naphthyl	$1{\cdot}9912x - 6{\cdot}1579y + 3{\cdot}4203z + 4{\cdot}1919 = 0$	0·012
Amide	$12{\cdot}1004x - 3{\cdot}2963y - 0{\cdot}2687z - 7{\cdot}5978 = 0$	0·007
	(*RS*)-ACE NAPH	
Naphthyl	$-4{\cdot}7142x + 6{\cdot}1285y + 6{\cdot}3056z - 1{\cdot}7975 = 0$	0·023
Amide	$-6{\cdot}8984x - 1{\cdot}9612y - 3{\cdot}7050z + 2{\cdot}8577 = 0$	0·021

* Only the C, N, O and F atoms were used to determine the best plane.
† $\sum \Delta^2$ is the sum of the squares of the deviations (in Å) of the n atoms forming the plane from the best plane.

Table 8. *Torsion angles* (°)

Atom group* *A—B—C—D*	(*R*)-TFA NAPH	(*R*)-ACE NAPH	(*RS*)-ACE NAPH†
C(13)—N—C(11)—C(1)	142·7 (4)	135·0 (5)	93·1 (9)
C(13)—N—C(11)—H(9)	30 (3)	18 (2)	−26
C(13)—N—C(11)—C(12)	−88·1 (6)	−97·4 (6)	−140·6 (7)
N—C(13)—C(14)—H(13)		−13 (4)	34
N—C(13)—C(14)—H(14)		−136 (5)	152
N—C(13)—C(14)—H(15)		123 (3)	−88
C(14)—C(13)—N—C(11)	176·7 (4)	178·8 (4)	176·3 (6)
N—C(11)—C(1)—C(2)	114·3 (5)	108·8 (5)	18 (1)
C(12)—C(11)—C(1)—C(2)	−11·3 (7)	−15·7 (8)	−105·5 (7)
N—C(13)—C(14)—F(1)	2·7 (7)		
N—C(13)—C(14)—F(2)	−113·4 (5)		
N—C(13)—C(14)—F(3)	125·9 (5)		

* The notation used for the torsion angle *A—B—C—D*: viewed along the vector *B* → *C*, the angle is zero when *A* and *D* are eclipsed. A positive angle designates clock wise rotation of the *C—D* bond with respect to the *A—B* bond.
† The torsion angles refer to a molecule of *R* configuration.

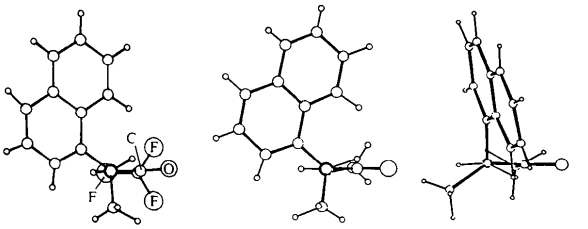

(*a*) (*b*) (*c*)

Fig. 1. Newman projection along the C(chiral)—N bond. (*a*) (*R*)-TFA NAPH, (*b*) (*R*)-ACE NAPH, (*c*) (*RS*)-ACE NAPH.

The conformations about the chiral atom are shown in Newman projections in Fig. 1. The C(chiral)—H bond is closest to being eclipsed with the OC—N bond in the three structures (Table 8).

The conformations of the two chiral molecules are almost identical and are decidedly different from that in the racemic crystal (Table 8, Fig. 1).

3. Molecular packing modes

3.1. *Possible* H-*bonding motifs*

H-bonds between *trans* mono-*N*-substituted primary amides, $R_C CONHR_N$, may be formed in various geometric patterns, determined by the nature of the residues attached to the amide group. The H-bonding motifs are classified here according to the symmetry elements that generate them, which are either chiral or achiral. These motifs are described below for chiral and racemic crystals.

3.1.1. *Chiral crystals.* The molecules may form H-bonds in several modes. One way is by translation which involves an axis approximately 5 Å long, a distance which is determined by the geometry of the amide group and the N—H···O bond (Fig. 2). This motif is unfavourable when either the R_C or R_N groups are bulky.

Another mode relating H-bonded molecules is *via* an *n*-fold screw axis. Three- and fourfold screw axes demand high-symmetry space groups, which are not generally consistent with close packing (Kitaigorodskii,

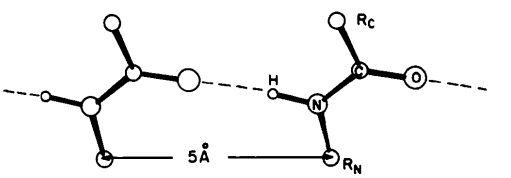

Fig. 2. H-bonding by 5 Å translation.

1973); these modes are therefore less probable. Nevertheless, whenever there is a necessity to reduce steric hindrance, the fourfold screw axis is a useful mode, in chiral crystals, for generating a H-bonded array in which R_C and R_N groups avoid each other by virtue of 90° rotation (Fig. 3). The molecules within the array may be related by a pseudo 4_1 axis, so as to avoid overall tetragonal symmetry, as discussed in § 3.2. The twofold screw-axis symmetry element has an advantage if the two substituents of the amide group are very different in size, for R_C and R_N would then alternate along the axis (Fig. 4), and minimize steric hindrance.

The n-fold screw axis involves a rotation angle of $(2\pi/n)$ followed by a translation of (t/n), where t is the axial length. Two H-bonded amide groups should be separated by about 5 Å along the screw axis and therefore this axis should be $\sim n \times 5$ Å long, which identifies the H-bonding motif when only cell constants are known.

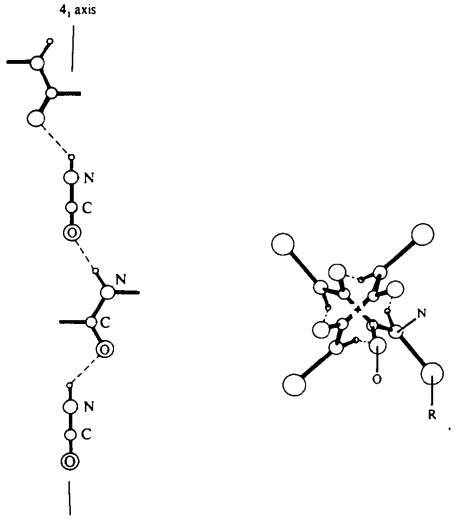

(*a*) (*b*)

Fig. 3. H-bonding by a fourfold screw axis as viewed: (*a*) perpendicular to the axis; (*b*) along the axis.

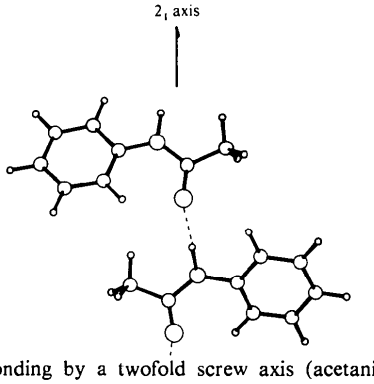

Fig. 4. H-bonding by a twofold screw axis (acetanilide; Brown, 1966).

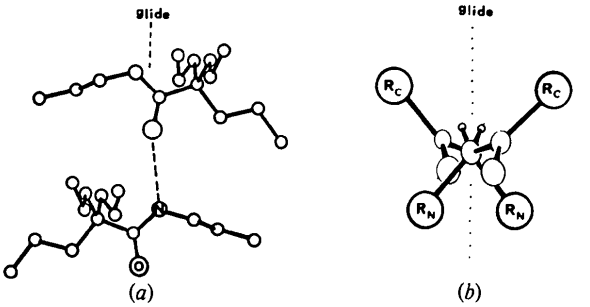

(*a*) (*b*)

Fig. 5. H-bonding by a glide plane. (*a*) Amide plane ~90° to glide plane; viewed perpendicular to glide axis [*N*-(*n*-propyl)tri-*n*-propylacetamide, Cohen-Addad & Grand, 1974]. (*b*) Amide plane ~45° to glide plane; viewed along the glide axis.

3.1.2. *Racemic crystals.* Racemic crystals may contain H-bonding motifs generated by achiral as well as chiral symmetry elements. From the achiral symmetry elements only the glide plane has to be considered for *trans* mono-*N*-substituted primary amides.

The glide plane may generate H-bonds and achieve close packing for R_C and R_N groups of various shapes and dimensions. When these groups are markedly different in size, the amide plane will be 90° to the glide plane (Fig. 5*a*) and, when both are bulky, the corresponding angle will be ~45° (Fig. 5*b*).

3.2. *The* H-*bonding motifs derived from cell constants*

The cell constants of enantiomerically pure and racemic amides RCONHCH(CH_3)Ar, where R = CH_3, CF_3, n-C_3H_7, n-$C_{11}H_{23}$ and $C(CH_3)_3$ and

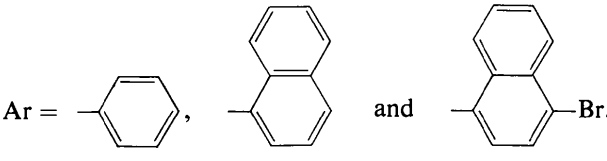

were determined and permit the identification of the symmetry elements that generate the H-bonds (Table 1). The H-bonding motifs are correlated with the nature of the groups attached to the amide function in the following analysis.

Of the thirteen amides in which R is unbranched (*i.e.* CH_3, CF_3, n-C_3H_7, n-$C_{11}H_{23}$), nine form H-bonded stacks along the 5 Å axis despite the presence of bulky CH(CH_3)Ar groups. H-bonding along either a twofold screw axis or a glide plane would have generated a more even packing on both sides of the amide stack. However, the translation mode is dominant. Only four compounds form H-bonds in a mode other than a 5 Å translation: (*R*)-ACE PHE forms H-bonds along a twofold screw axis which is parallel to the diagonal

$a + b$ of length 9·6 Å; three racemic amides, namely one modification of (*RS*)-ACE NAPH, (*RS*)-TFA NAPH and (*RS*)-*N*-lauroyl-1-(1-naphthyl)ethylamine [(*RS*)-LAU NAPH], form H-bonded arrays along a glide plane of 9 Å.

Compounds in which R_C is the bulky *tert*-butyl group cannot form H-bonds by 5 Å translation because of steric hindrance (as can also be seen from CPK models). Thus, (*S*)-*N*-pivaloyl-1-phenylethylamine [(*S*)-PIVA PHE], with a bulky R_C group, forms H-bonds along a fourfold screw axis of 19·7 Å (Fig. 3). In (*S*)-PIVA NAPH three twofold screw axes are observed, but none of their lengths corresponds to H-bonding about a 2_1 axis. One reasonable way to account for H-bonding is by a pseudo-fourfold screw axis. There are two independent molecules in the asymmetric unit, which are probably related by a pseudo fourfold screw axis along the 19 Å axis (either *a* or *c*), leading to an array whose fourfold screw symmetry is limited to the H-bonding system and is not part of the overall crystal symmetry. There are many known examples in which the symmetry of the H-bonded array is higher than that of the overall crystal symmetry (Harada & Iitaka, 1974; Leiserowitz, 1976; von Hechtfischer, Steigemann & Hoppe, 1976; Bernstein & Leiserowitz, 1972). This stems from the need for close packing, which does not normally conform with high crystal symmetry, and simultaneous maintenance of the favourable H-bonding motif.

The H-bonding modes of the respective racemates of the two compounds described above cannot be unambiguously deduced from their cell constants. (*RS*)-PIVA PHE has two molecules in the asymmetric unit. Either it is H-bonded along the 9·5 Å twofold screw axis or *R* and *S* molecules are bonded along a pseudo glide plane of 9·5 Å. The H-bond motif of (*RS*)-PIVA NAPH cannot be deduced from its triclinic cell constants.

The frequency of the 5 Å translation motif indicates that the intermolecular contacts between $CH(CH_3)Ar$ groups of the same chirality, as well as contacts between the *R* groups when generated by translation, impart additional stability to the H-bonded structure.

Table 9. *The geometry of the* H-*bond*

	(*R*)-TFA NAPH	(*R*)-ACE NAPH	(*RS*)-ACE NAPH
N—H···O distance (Å)	3·01	2·89	2·87
C—O···N angle (°)	176·2	167·6	136·0
C—N···O angle (°)	129·8	112·2	122·5
Deviations of N and H atoms from plane of amide group to which the N—H is H-bonded (Å)	0·06, 0·1	0·26, 0·3	1·95, 1·3

3.3. *Molecular packing of* (*R*)-*TFA NAPH,* (*R*)-*ACE NAPH and* (*RS*)-*ACE NAPH*

The crystal structures of (*R*)-*N*-trifluoroacetyl-1-(1-naphthyl)ethylamine and (*R*)-*N*-acetyl-1-(1-naphthyl)ethylamine were determined to ascertain the H-bonding as well as other interactions involved in the 5 Å translational motif. We also determined the structure of (*RS*)-*N*-acetyl-1-(1-naphthyl)ethylamine

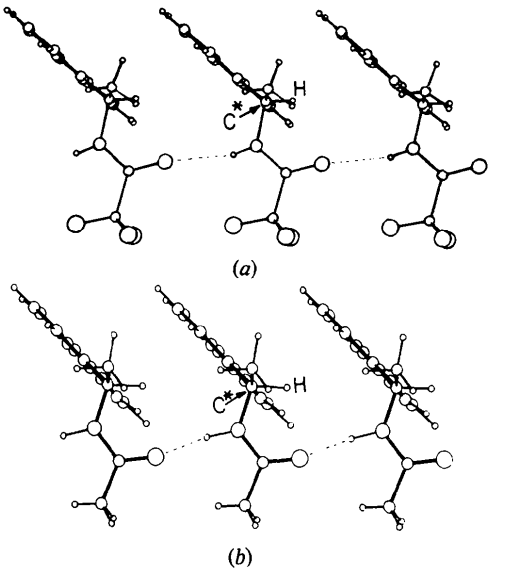

Fig. 6. H-bonding by 5 Å translation viewed perpendicular to the amide plane (*a*) (*R*)-TFA NAPH, (*b*) (*R*)-ACE NAPH.

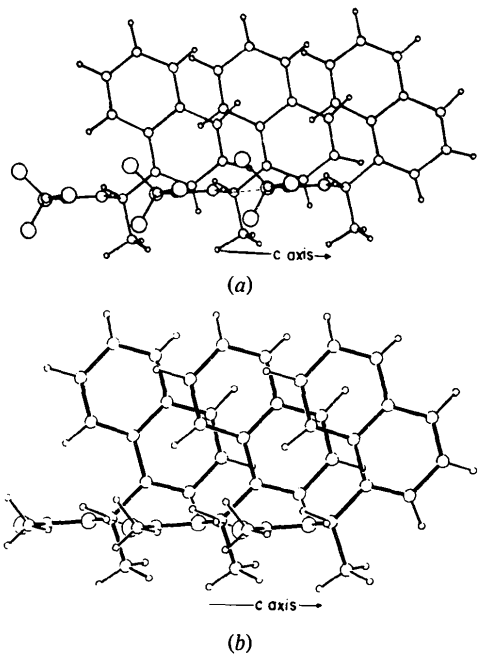

Fig. 7. Overlap between naphthyl groups viewed perpendicular to naphthyl plane. (*a*) (*R*)-TFA NAPH, (*b*) (*R*)-ACE NAPH.

which forms H-bonds by a glide plane so that the translation and glide-plane motifs could be compared. The H-bonding geometry in the three crystals is given in Table 9.

The H-bonding array in the two chiral crystals is generated by a 5 Å translation (Fig. 6). Within this array the naphthyl rings make plane-to-plane contacts of 3·4 Å. Their overlap is shown in Fig. 7.

A noteworthy feature within this arrangement is that the H atom linked to the chiral C atom is wedged between two naphthyl planes, making a close contact of 2·8 and 2·6 Å with C(2) of the neighbouring naphthyl rings in (*R*)-TFA NAPH and (*R*)-ACE NAPH, respectively (Fig. 6). In contrast, the methyl group attached to the chiral C atom points away from the stack, and thus does not participate in any short intrastack contacts (Fig. 7).

(*RS*)-ACE NAPH makes linear N—H···O bonds along a glide plane of 9·0 Å axial length (Fig. 8). The planes of the amide groups engaged in H-bonding make an angle of 130° with each other such that the N—H bond is directed towards the O atom from well above the amide plane (Table 9). This type of H-bonding arrangement is rarely observed, one example being urea (Sklar, Senko & Post, 1961).

A quantitative comparison of the packing energies of the two H-bonding arrays comprising molecules interlinked by 5 Å translation and by the glide plane is given below (§ 3.5).

The interstack packings in the two chiral structures display a herring-bone arrangement of the naphthyl groups related by the twofold screw axis (Fig. 9). This feature is commonly observed in crystals of aromatic hydrocarbons (Bacon, Curry & Wilson, 1964; Abrahams, Robertson & White, 1949; Mason, 1964).

Regarding the racemic crystal, the structure exhibits herring-bone contacts between glide-related naphthyl rings (Fig. 10).

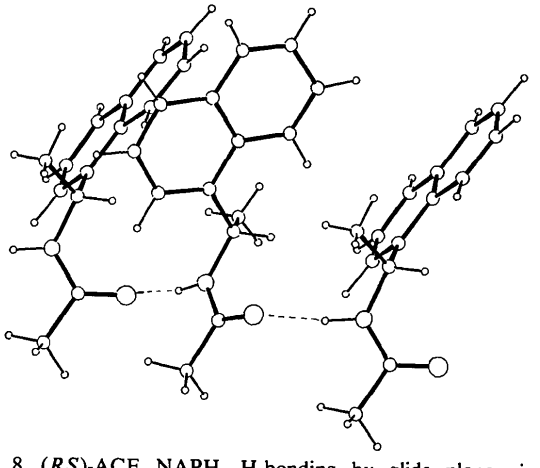

Fig. 8. (*RS*)-ACE NAPH. H-bonding by glide plane viewed perpendicular to the amide planes of the outer molecules.

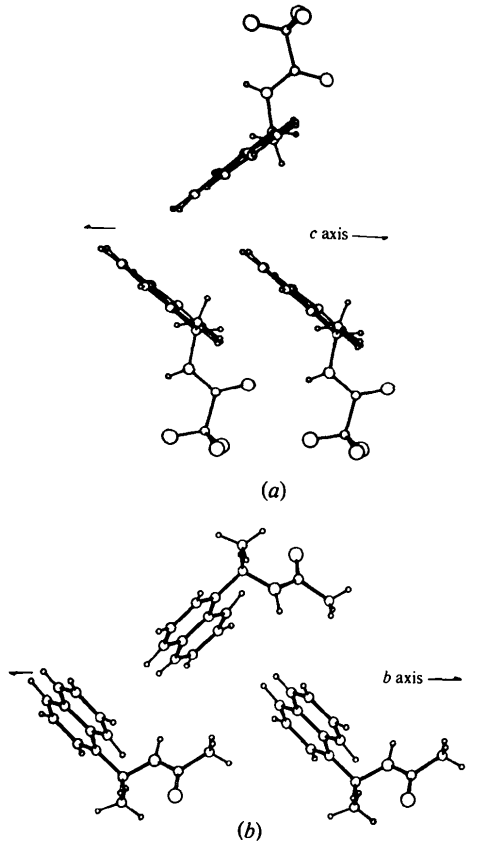

Fig. 9. Herring-bone packing. (*a*) (*R*)-TFA NAPH, (*b*) (*R*)-ACE NAPH.

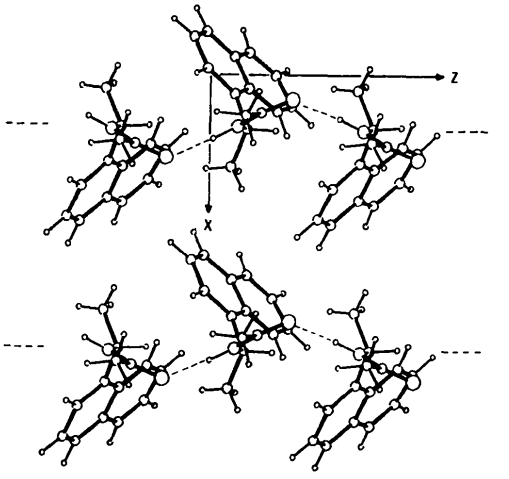

Fig. 10. (*RS*)-ACE NAPH. H-bonding and herring-bone packing by a glide plane, viewed perpendicular to the *ac* plane.

3.4. *Packing arrangement of* (*R*)-*LAU PHE*, (*RS*)-*LAU NAPH*, (*R*)-*LAU NAPH*Br *and* (*R*)-*LAU NAPH*

Solution of the crystal structures of (*R*)-TFA NAPH, (*R*)-ACE NAPH and (*RS*)-ACE NAPH has enabled us to deduce the packing features of some of

the other mono-*N*-substituted primary amides, given only their cell constants (Table 1).

3.4.1. *(R)-N-Lauroyl-1-phenylethylamine* [*(R)-LAU-PHE*]. The crystals contain 2 molecules per unit cell in space group $P2_12_12$. Therefore, the molecules must lie on the twofold axis in a disordered manner as the molecule itself does not possess twofold symmetry. The molecules are H-bonded along the 5 Å *a* axis to form ribbons. Within these ribbons the parallel aliphatic chains are in close contact with each other. The interribbon contact between aliphatic chains along *b* (7·6 Å) is achieved by the twofold screw axis at $y = \frac{1}{4}$, $z = \frac{1}{2}$ (Fig. 11), such that the separation between these chains is $b/2 = 3{\cdot}8$ Å; this postulate is supported by the intense 020 and 040 reflections in the X-ray diffraction photographs. Moreover, the length of the extended molecule is approximately 23 Å, and the length of *c* is 26 Å. Therefore, the molecular axis along the carbon chain must be almost coincident with the crystallographic twofold axis. To achieve maximum interribbon contacts between hydrocarbon chains and acceptable overall packing, the chain centres must be positioned at $z \simeq \frac{1}{2}$. This arrangement generates a (001) layer, the thickness of which is approximately the length of the molecule. The number of intermolecular van der Waals contacts is much higher within the (001) layer than between layers. Therefore, the disorder, inducing apparent twofold molecular symmetry, can only exist between layers. This proposed disorder between layers must be random, since there is no indication of X-ray diffuse scattering.

3.4.2. *(RS)-N-Lauroyl-1-(1-naphthyl)ethylamine* [*(RS)-LAU NAPH*]. The cell constants are very similar to those of (*RS*)-ACE NAPH, the crystal structure of which was determined, except for the longer *b* axis (29·6 *vs* 17·4 Å), which accommodates the long hydrocarbon chain. Consequently, the packing arrangement (Fig. 12) can be deduced from that of the acetyl analogue by simply adding an extended hydrocarbon chain. The central axis of the lauroyl chain lies very close to the *c*-glide plane. The twofold screw axis

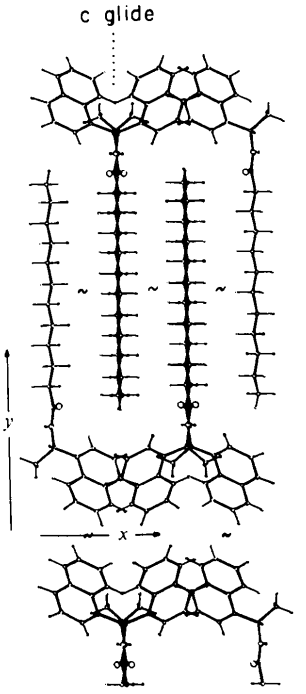

Fig. 12. Postulated packing arrangement of (*RS*)-LAU NAPH viewed along the H-bonding axis.

at $y = \frac{1}{2}$ generates interstack contacts between the hydrocarbon chains spaced 4 Å along the *a* axis; the twofold screw axis at $y = 0$ generates contacts between naphthyl groups as in (*RS*)-ACE NAPH. This deduced packing arrangement demonstrates how both H-bonding and hydrocarbon-chain overlap can occur between molecules related by a glide plane. The glide-plane operation becomes a pseudo-translation of half an axial length ($c/2 = 4{\cdot}6$ Å) with regard to the carbon chains by virtue of their mirror symmetry whose plane is located very close to the crystallographic glide plane.

3.4.3. *(R)-Lauroyl-1-[1-(4-bromonaphthyl)]ethylamine* [*(R)-LAU NAPH*Br]. The postulated packing arrangement is shown in Fig. 13. The molecules form H-bonded stacks along the 5 Å axis. These stacks are

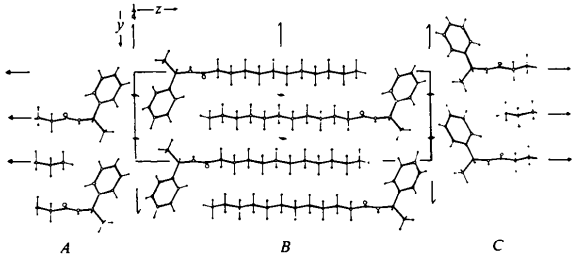

Fig. 11. Postulated packing arrangement of (*R*)-LAU PHE viewed along the H-bonding *a* axis. Layers *A* and *B* are related by translation. Layer *C* is related to *A* and *B* by the crystallographic twofold axis.

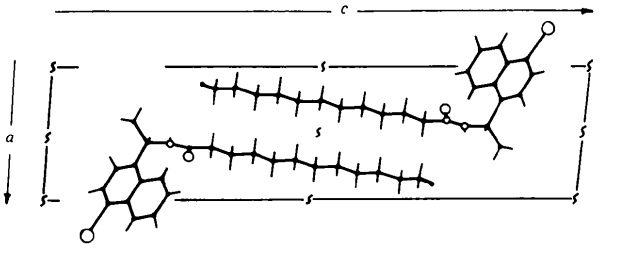

Fig. 13. Postulated packing arrangement of (*R*)-LAU NAPHBr viewed along the H-bonding axis.

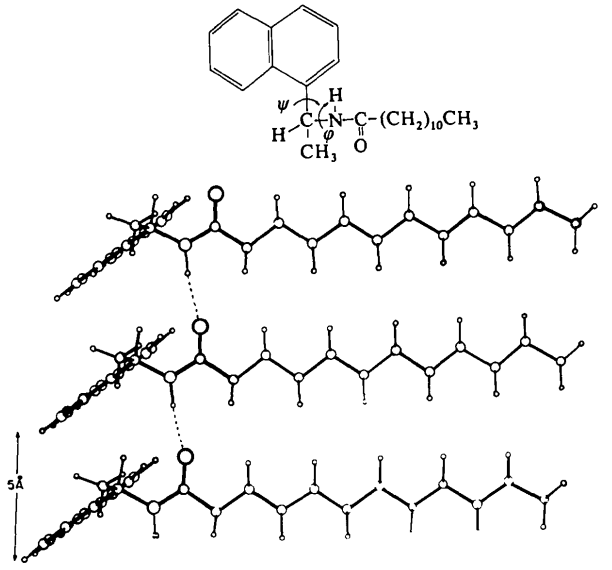

Fig. 14. Postulated packing arrangement of (*R*)-LAU NAPH viewed perpendicular to amide plane.

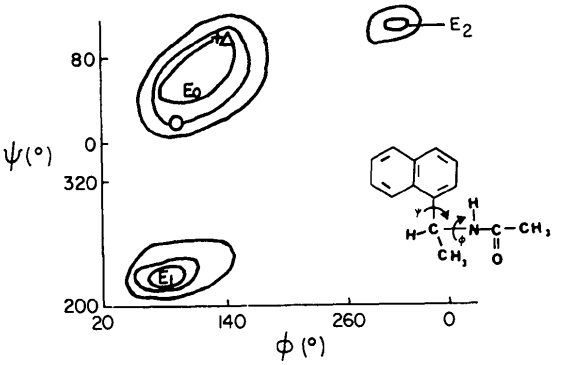

Fig. 15. Molecular-energy surface of *N*-acetyl-1-(1-naphthyl)ethylamine as a function of φ and ψ. The lowest energy contours are indicated by E_0, E_1, E_2. $E_1 = E_2 = E_0 + 25$ kJ mol^{-1}. Contour interval is 12·5 kJ mol^{-1}. The symbols △, +, and O indicate the φ and ψ values found in the crystals of (*R*)-TFA NAPH, (*R*)-ACE NAPH and (*RS*)-ACE NAPH, respectively.

placed parallel to the (102) plane, the diffraction from which is very intense. Interstack distances of approximately 3·8 Å between aliphatic chains are achieved across the two twofold screw axes at $x = \frac{1}{2}$, $z = 0$ and $x = \frac{1}{2}$, $z = \frac{1}{2}$.

3.4.4. (*R*)-*N*-*Lauroyl*-1-(1-*naphthyl*)*ethylamine* [(*R*)-*LAU NAPH*]. Single crystals suitable for determination of full cell constants could not be obtained. An X-ray oscillation photograph, however, did show the existence of a 5 Å axis, and with this limited information the H-bonding mode was revealed (Fig. 14). The powder diffraction pattern exhibits reflections that may correspond to a 30 Å axis which probably accommodates the length of the molecule. By comparison, the long axis of (*RS*)-LAU NAPH is 29·6, and that of (*R*)-LAU NAPHBr 30·9 Å.

3.5. *Conformation and packing analysis by energy computations*

Energy computations were undertaken to determine the most stable molecular conformations, and to evaluate the relative stability of translation and glide-plane packing modes for various molecular conformations. Torsion and van der Waals non-bonded energy terms using pairwise atom–atom potentials were computed by the *QCFF/PI* computer program (Warshel & Karplus, 1972; Warshel & Levitt, 1974; Warshel & Lifson, 1970).

The energy of a single molecule of *N*-acetyl-1-(1-naphthyl)ethylamine, whose atomic coordinates were taken from the chiral crystal structure, was calculated as a function of its conformation. The conformation was varied by rotations of φ[C(13)–N–C(11)–C(1)] and ψ[N–C(11)–C(1)–C(2)] defined in Table 8 and Fig. 15. The whole φ,ψ range was covered in increments of 30°. The energy map (Fig. 15) contains three minima. The lowest minimum E_0 encompasses, very close to its innermost contour, the conformations observed in the three structures: (*R*)-*N*-trifluoroacetyl-1-(1-naphthyl)ethylamine and (*R*)- and (*RS*)-*N*-acetyl-1-(1-naphthyl)ethylamine (Table 8).

Energies of the H-bonded arrays were then calculated. Positive energy values were obtained for intermolecular interactions. The amide H and O atoms participating in the N–H···O bond were treated as an alkyl H atom and C atom respectively and so the short (N)H···O distance of ~1·9 Å led to apparent strong repulsion. Moreover, the attractive electrostatic forces, which are rather significant for N–H···O bonds, were not considered. Thus, though the energies obtained are all high by a constant value, the comparative study is reliable. This is due to the fact that the H-bonds are kept fixed throughout the calculation of the 5 Å translation mode and there is only a small difference in electrostatic energy, of 2 kJ mol^{-1}, between the translation mode and the glide-plane mode of H-bonding (Berkovitch-Yellin & Leiserowitz, 1980). To evaluate the relative stability of translation and glide-plane packing for various molecular conformations, we considered only a trimer of molecules in the H-bonded array to represent the H-bonded stack for we only considered nearest-neighbour contacts. The boundary values of φ, 60 to 180°, and of ψ, 0 to 120°, were chosen to encompass the region of stable conformations (Fig. 15).

3 5.1. *The* H-*bonded translation stack.* This structure consists of three molecules related by a 5 Å

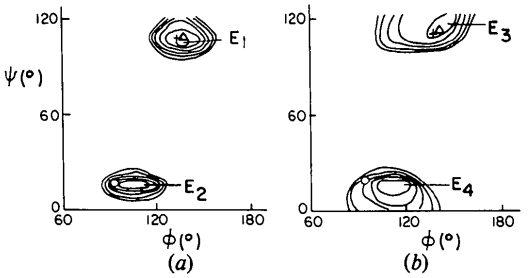

Fig. 16. Variation in energy as a function of φ and ψ of three molecules of (*R*)-ACE NAPH related by 5 Å translation. Lowest energy-contour values are indicated by E_1, E_2, E_3, E_4, where $E_2 = E_1 + 25$ kJ mol^{-1} and $E_4 = E_3$. Contour interval is 8·4 kJ mol^{-1}. (*a*) Total (inter- + intramolecular) energy. (*b*) Intermolecular energy. The symbols △, + and O indicate φ and ψ torsion angles in crystalline (*R*)-TFA NAPH, (*R*)-ACE NAPH and (*RS*)-ACE NAPH, respectively.

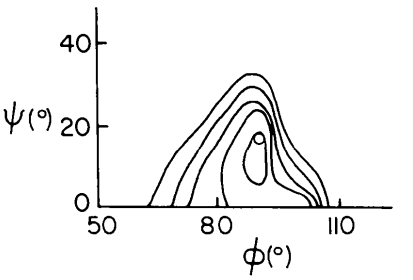

Fig. 17. Variation in intermolecular energy as a function of φ and ψ of three molecules of ACE-NAPH related by a glide plane. Contour interval is 8·4 kJ mol^{-1}. O Indicates the φ and ψ values found in the crystal of (*RS*)-ACE NAPH.

translation whose amide groups are related as in the crystal. The conformation was varied by incrementing φ and ψ by 10° maintaining translation symmetry, and the energy of each resulting structure was calculated. Fig. 16(*a*) shows the map for the combined intra- and intermolecular energy of the trimer. Fig. 16(*b*) shows the intermolecular non-bonded energy only. The molecular conformation experimentally found in (*R*)-TFA NAPH falls within the lowest energy contour. Trimers constructed from molecules with conformations corresponding to the other two minima of Fig. 15 resulted in interpenetration of naphthyl groups.

Thus, it can be concluded that the 5 Å translation stack with the molecular conformation as found in the crystal is the most stable. This is also in keeping with the fact that the molecular conformation and the H-bonded arrays of (*R*)-TFA NAPH and (*R*)-ACE NAPH are almost identical despite their different overall packing arrangements.

3.5.2. *The* H-*bonded glide-plane stack*. This structure consists of three molecules related by a glide plane. The geometry of H-bonding was taken as observed in the racemic crystal structure of (*RS*)-ACE NAPH. The conformation of the molecules was varied by incrementing φ and ψ by 10° maintaining glide-plane symmetry, and the energy of each structure was calculated. The results are given in Fig. 17. The φ and ψ values corresponding to the molecular conformation found in the racemic crystal [(*RS*)-ACE NAPH] are located within the lowest contour.

These calculations indicate that the 5 Å translation stack is more stable than the glide-plane-related array by 38 kJ mol^{-1}. The value of 38 kJ mol^{-1} in favour of the translation motif seems too high. Nevertheless, the difference is partly accounted for by aromatic overlap and other interactions which are present in the translation stack but are absent in the glide-plane stack. In the crystal the glide-plane packing is compensated for by interstack contacts.

3.6. *Contacts in the* 5 Å *translation array*

The 5 Å translation mode fulfils the requirements for H-bonding and for close packing between the aromatic residues linked to the chiral C atom. It is also of interest to consider the relative contribution of contacts between long aliphatic chains of acyl groups, when present, to the stability of the stack.

In the crystal structure of the *N*,*N*-substituted primary diamide *N*,*N*′-hexamethylenebispropionamide (Jensen, 1962), the molecules interlinked by H-bonds along a 5 Å axis make close contacts of 3·7–4·0 Å between nearest-neighbour C atoms. Thus the *N*-substituted primary amides containing aliphatic chains H-bonded along a 5 Å axis make 4 Å contacts between the C atoms of the neighbouring acyl chains.

Close packing between parallel aliphatic chains has been observed in paraffins (Kitaigorodskii, 1973; Norman & Mathisen, 1961*a*,*b*; Mathisen, Norman & Pedersen, 1967), carboxylic acids (Lomer, 1963; Larssen & von Sydow, 1966; Malta, Celotti, Zanetti & Martelli, 1971), their esters (Aleby, 1968) and amides (Turner & Lingafelter, 1955*a*,*b*). The straight-chain aliphatic primary amides from propanamide to hexadecanamide (Turner & Lingafelter, 1955*a*,*b*) all pack with a distance of 4·1 Å between parallel chains. The relative contribution of H-bonding and aliphatic-chain contacts to structural ability has been evaluated in some cases. One example is provided by the crystal structures of D- and DL-2-methyloctadecanoic acid (Abrahamsson, 1959*a*,*b*). The carboxyl groups in the racemic crystal form cyclic H-bonded dimers across centres of inversion and the aliphatic chains are closely packed along a 5 Å axis. The aliphatic chains in the chiral crystal pack as well by translation along a 5 Å axis, which in this structure also acts as a twofold screw axis to generate the H-bonds. This short twofold screw axis induces a distorted H-bonding system (Leiserowitz, 1976), the only reported example of its kind. The arrangement is indicative of the adjustment of the structure to the requirements of close packing of the aliphatic chains.

Another example is given by 1-decyl-α-D-glucopyranoside (Moews & Knox, 1976) which packs along a 5 Å axis. The molecules form both H-bonds and contacts between aliphatic chains along this axis. The authors observed that the hydrocarbon packing appeared to be more 'perfect' than the H-bonding; the chains were 'very closely packed' whereas most of the H-bonds 'severely deviated from linearity'.

3.7. *Structure of the mono-N-substituted primary amides in the liquid state*

The marked stability of the 5 Å translation array of RCONHCH(CH_3)Ar in the solid state led us to search for similar packing features in the liquid phase. Knowledge of their structure in the liquid is particularly relevant to interactions of optically active substrates with these amides acting as chiral stationary phases in separation of enantiomers by gas–liquid chromatography (Weinstein, Feibush & Gil-Av, 1976).

The maintenance of order in the liquid phase has been demonstrated in a number of pertinent systems. The similarity of the average molecular arrangement of benzene in the liquid to the packing in the crystalline phase has been established by X-ray scattering (Katzoff, 1934; Narten, 1968). There is also evidence, both direct (X-ray scattering) (Katzoff, 1934) and indirect (Mumford, 1952; Seyer, Patterson & Keays, 1944; Vand, 1953; Champion & Meeten, 1968; Moore, Gibbs & Eyring, 1953) for close packing between parallel chains in liquid *n*-alkanes.

Encouraged by their results we have measured the X-ray scattering by melted (*R*)-LAU NAPH, (*R*)-TFA NAPH, and (*R*)-PIVA NAPH, compounds used in the gas–liquid chromatographic resolutions (Weinstein, Feibush & Gil-Av, 1976). X-ray-scattering photographs of (*R*)-LAU NAPH, (*R*)-TFA NAPH, (*R*)-PIVA NAPH and *n*-heptane in the melted phase were taken on a Debye–Scherrer camera with Cu $K\alpha$ radiation. The samples were sealed in 1 mm Lindemann-glass capillaries (wall thickness 0·01 mm), heated a few degrees above melting point and irradiated for 20 h. The intensities were measured on a Joyce–Loebel microdensitometer. The Bragg intensities, as a function of θ, are shown in Fig. 18. The d spacings of the reflections [$1{\cdot}2\lambda/2\sin\theta$ (Guinier, 1952), as compared with the Bragg formula $\lambda/2\sin\theta$] correspond to a distance which frequently occurs between the molecules. The X-ray intensity disitributions have the following characteristics. The sharpest and strongest peak is exhibited by (*R*)-LAU NAPH with a d spacing of 5·4 Å. The peak of (*R*)-TFA NAPH is more diffuse and its maximum intensity lies at the same d value (5·3 Å). (*R*)-PIVA NAPH exhibits the most diffuse and weakest peak and its maximum is located at a significantly larger value of 6·1 Å.

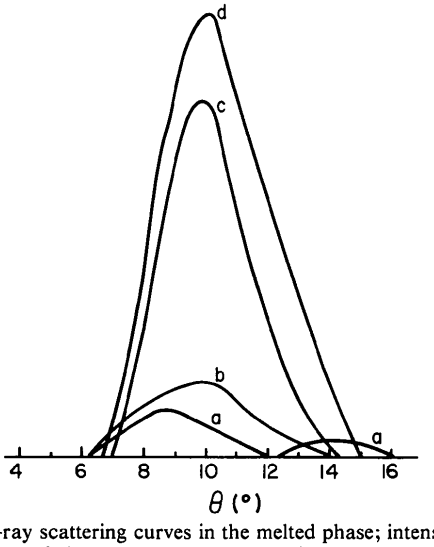

Fig. 18. X-ray scattering curves in the melted phase; intensity as a function of θ (Cu $K\alpha$ radiation). (*a*) (*R*)-PIVA NAPH, (*b*) (*R*)-TFA NAPH, (*c*) (*R*)-LAU NAPH, (*d*) *n*-heptane.

The d spacings of (*R*)-LAU NAPH and (*R*)-TFA NAPH are compatible with the H-bonding translation of 5 Å found in their crystalline phases. The more intense peak of (*R*)-LAU NAPH may be ascribed to an abundance of 5 Å distances between parallel aliphatic chains. Since the scattering of *n*-heptane had been measured and interpreted by Katzoff (1934) to stem from close packing of parallel chains, this compound was measured as a reference. Its peak position (Fig. 18) was found to be very similar to that of (*R*)-LAU NAPH and (*R*)-TFA NAPH. The larger d spacing observed in (*R*)-PIVA NAPH appears to be in agreement with H-bonds generated by a fourfold screw axis as found in the crystal, in which two molecules are at right angles to each other. This results in an average interatomic distance between the molecules larger than in the 5 Å translation array.

These measurements indicate that the packing features of the 5 Å translation stack in the crystal are, at least partially, preserved in the liquid phase.

The molecular packing in the series of mono-*N*-substituted primary amides analysed here has been used to account for various facets of chiral recognition in the solid state and in the melt (Weinstein, Leiserowitz & Gil-Av, 1980).

We thank Sara Ariel, C. P. Tang and Y. Halfon for assistance in X-ray measurements.

References

ABRAHAMS, S. C., ROBERTSON, J. M. & WHITE, J. G. (1949). *Acta Cryst.* **2**, 233–238.
ABRAHAMSSON, S. (1959*a*). *Acta Cryst.* **12**, 301–304.
ABRAHAMSSON, S. (1959*b*). *Acta Cryst.* **12**, 304–309.
ALEBY, A. (1968). *Acta Chem. Scand.* **22**, 811–818.

BACON, G. E., CURRY, N. A. & WILSON, S. A. (1964). *Proc. R. Soc. London Ser. A*, **279**, 98–110.
BERKOVITCH-YELLIN, Z. & LEISEROWITZ, L. (1980). *J. Am. Chem. Soc.* Submitted.
BERNSTEIN, J. & LEISEROWITZ, L. (1972). *Isr. J. Chem.* **10**, 601–612.
BROWN, C. J. (1966). *Acta Cryst.* **21**, 442–445.
CHAMPION, J. V. & MEETEN, G. H. (1968). *Trans. Faraday Soc.* **64**, 238–247.
COHEN-ADDAD, C. & GRAND, A. (1974). *Acta Cryst.* B**30**, 186–192.
COPPENS, P., LEISEROWITZ, L. & RABINOVICH, D. (1965). *Acta Cryst.* **18**, 1035–1038.
GERMAIN, G., MAIN, P. & WOOLFSON, M. M. (1971). *Acta Cryst.* A**27**, 368–376.
GUINIER, A. (1952). *X-ray Crystallographic Technology*, p. 253. London: Hilger & Watts.
HAGLER, A. T., LEISEROWITZ, L. & TUVAL, M. (1976). *J. Am. Chem. Soc.* **98**, 4600–4612.
HARADA, Y. & IITAKA, Y. (1974). *Acta Cryst.* B**30**, 1452–1459.
HECHTFISCHER, S. VON, STEIGEMANN, W. & HOPPE, W. (1976). *Acta Cryst.* B**26**, 1713–1722.
International Tables for X-ray Crystallography (1962). Vol. III, pp. 202–203. Birmingham: Kynoch Press.
JENSEN, L. H. (1962). *Acta Cryst.* **15**, 433–440.
KATZOFF, S. (1934). *J. Chem. Phys.* **2**, 841–851.
KITAIGORODSKII, A. I. (1973). *Molecular Crystals and Molecules*. New York: Academic Press.
LAHAV, M., LAUB, F., GATI, E., LEISEROWITZ, L. & LUDMER, Z. (1976). *J. Am. Chem. Soc.* **98**, 1620–1622.
LARSSEN, K. & VON SYDOW, E. (1966). *Acta Chem. Scand.* **20**, 1203–1207.
LEISEROWITZ, L. (1976). *Acta Cryst.* B**32**, 775–802.
LOMER, T. R. (1963). *Acta Cryst.* **16**, 984–988.
MALTA, V., CELOTTI, G., ZANNETTI, R. & MARTELLI, A. F. (1971). *J. Chem. Soc. B*, pp. 548–553.
MASON, R. (1964). *Acta Cryst.* **17**, 547–555.
MATHISEN, H., NORMAN, N. & PEDERSEN, B. F. (1967). *Acta Chem. Scand.* **21**, 127–135.
MOEWS, P. C. & KNOX, J. R. (1976). *J. Am. Chem. Soc.* **98**, 6628–6633.
MOORE, R. J., GIBBS, P. & EYRING, H. (1953). *J. Phys. Chem.* **57**, 172–178.
MUMFORD, S. A. (1952). *J. Chem. Soc.* pp. 4897–4913.
NARTEN, A. H. (1968). *J. Chem. Phys.* **48**, 1630–1634.
NORMAN, M. & MATHISEN, H. (1961*a*). *Acta Chem. Scand.* **15**, 1747–1754.
NORMAN, M. & MATHISEN, H. (1961*b*). *Acta Chem. Scand.* **15**, 1755–1760.
SEYER, W. F., PATTERSON, R. F. & KEAYS, J. L. (1944). *J. Am. Chem. Soc.* **66**, 179–182.
SKLAR, N., SENKO, M. E. & POST, B. (1961). *Acta Cryst.* **14**, 716–720.
TURNER, J. D. & LINGAFELTER, E. C. (1955*a*). *Acta Cryst.* **8**, 549–550.
TURNER, J. D. & LINGAFELTER, E. C. (1955*b*). *Acta Cryst.* **8**, 551–557.
VAND, V. (1953). *Acta Cryst.* **6**, 797–798.
WARSHEL, A. & KARPLUS, M. (1972). *J. Am. Chem. Soc.* **94**, 5613–5625.
WARSHEL, A. & LEVITT, M. (1974). *Quantum Chemistry Program Exchange* No. 247, Indiana Univ.
WARSHEL, A. & LIFSON, S. (1970). *J. Chem. Phys.* **53**, 582–594.
WEINSTEIN, S., FEIBUSH, B. & GIL-AV, E. (1976). *J. Chromatogr.* **126**, 97–111.
WEINSTEIN, S., LEISEROWITZ, L. & GIL-AV, E. (1980). *J. Am. Chem. Soc.* In the press.

Acta Cryst. (1980). B**36**, 1418–1424

Structures de Trois Produits de la Réduction Electrolytique du Cation Dibenzyl-1,4 Phényl-6 Dihydro-2,3 Diazépinium-1,4: Les Isomères *méso* et Racémique de la Bi-7 : 7′ (Dibenzyl-1,4 Phényl-6 Tétrahydro-1,2,3,4 Diazépine-1,4) et le Bis(dibenzyl-1,3 imidazolidinyl-2)-1,4 Diphényl-1,4 Butadiène-(1*Z*,3*E*)

PAR MAURICE VAN MEERSSCHE, GABRIEL GERMAIN ET JEAN-PAUL DECLERCQ

Laboratoire de Chimie Physique et de Cristallographie, Université de Louvain, place Louis Pasteur 1, *B*-1348 *Louvain-la-Neuve, Belgique*

(*Reçu le* 3 *septembre* 1979, *accepté le* 21 *janvier* 1980)

Abstract

The crystal structures of 7,7′-bi(1,4-dibenzyl-6-phenyl-1,2,3,4-tetrahydro-1,4-diazepine), *meso* (I) and racemic (II) isomers, and (1*Z*,3*E*)-1,4-bis(1,3-dibenzyl-2-imidazolidinyl)-1,4-diphenylbutadiene (III) have been solved by direct methods (*MULTAN*) from diffractometer data. The crystals are monoclinic, space group $C2/c$, with $a = 16{\cdot}978\,(3)$, $b = 11{\cdot}413\,(3)$, $c = 20{\cdot}371\,(7)$ Å, $\beta = 95{\cdot}64\,(2)°$ and $Z = 4$ for (I);

0567-7408/80/061418-07$01.00